Reaction Chemistry & Engineering

ROYAL SOCIETY OF CHEMISTRY

PAPER

View Article Online
View Journal | View Issue

Check for updates

Cite this: *React. Chem. Eng.*, 2026, 11, 334

Role of metal ion promoters in carbon nanotubes functionalization by polydopamine in the perspective of electroplated copper–carbon composites

Elisa Silva, [ac] Jérôme Guillot, [a] Patrick Grysan, [a] Damien Lenoble, [b] Emanuele Barborini [a] and Didier Arl *[a]

Received 7th May 2025,
Accepted 15th September 2025

DOI: 10.1039/d5re00209e

rsc.li/reaction-engineering

The present study investigates the sinergetic role of pH and metal ions promoters (Cu^{2+} and Ni^{2+}) in the tailoring of polydopamine (PDA) functionalization of carbon nanotubes (CNTs) with the ultimate goal of integration and control of copper matrix composites. We hereby demonstrate that mildly alkaline conditions combined with the presence of redox-active metal ions significantly enhance the yield of PDA coating on CNTs surface, by promoting dopamine polymerization *via* metal-assisted autoxidation and chelation mechanisms. The use of a catecholamine (PDA) coating and incorporation of metal promoters like copper and nickel enabled stability of the spraying solution. The effects of the CNTs surface modifications on the polymerization yield and electrical properties were evaluated. Although PDA reduces the functionalized CNTs conductivity due to its insulating nature, its role as a versatile interfacial layer is amplified in the presence of metal ions, which facilitate denser and more homogeneous polymer deposition. These findings reveal how surface modification enhances copper–carbon interfaces in CNT-based metal matrix composites, improving composite design and performance for lightweight applications requiring high current resistance, such as lightning strike protection in aircraft.

Introduction

Bringing electrical transport in polymer matrices through the inclusion of carbon nanostructures such as carbon nanotubes (CNTs) has been widely described in the literature.[1–7] Less has been done on studying the incorporation of CNTs in metals and more specifically the role of carbon–metal interfaces in the thermal/electrical transport. This aspect is crucial for antistatic or electrical discharge-related issues occurring in aeronautic applications. For instance, an airplane is predicted to be struck by lightning at least once a year on its commercial routes, with electrical discharges passing 200 000 amperes.[8,9] Such phenomenon poses a major risk to flight security, causing severe mechanical damage. Hence, prompting the development of highly efficient lightning strike protection systems can preserve the structural integrity of the plane. Copper, notable for its electrical and thermal conductivities, of 5.8×10^5 S cm^{-1} and 401 W m^{-1} K^{-1} at 27 °C respectively, is frequently used in lightning protection.[10] Copper high density poses, however, a great drawback on the performance of the airplane, as the additional copper elements increases the overall weight and therefore fuel consumption and carbon dioxide emissions. This issue has led the aviation sector to look into new materials that are capable of offering lightning protection while simultaneously being lightweight, in order to follow their sustainability plan.[11–13]

CNTs inclusion in metal matrix such as copper can significantly reduce the overall weight of the related composite while maintaining, or even enhancing, its electrical conductivity.[13] Subramaniam *et al.* described in 2013 the preparation of copper-CNT composites with one hundred fold increase in the ampacity, the maximum current a material can carry without overheating and suffering failure, compared to that of pure copper.[14] However, reproducing these results has proven difficult, the main reason being the cuprophobic and hydrophobic nature of CNTs, which hinders their wetting by metals like copper. This poor wettability leads to phase separation and inadequate dispersion, ultimately limiting the composite's electrical and mechanical performance.[11–15]

[a] *Luxembourg Institute of Science and Technology (LIST), Belvaux, L-4422, Luxembourg. E-mail: didier.arl@list.lu*
[b] *University of Luxembourg, 4365 Esch-Belval Esch-sur-Alzette, Luxembourg*
[c] *Department of Physics and Materials Science, University of Luxembourg, Esch-sur-Alzette, L-4365, Luxembourg*

To address this issue, recent efforts have been made to modify the CNT surface aiming to improve its interaction with copper. The covalent functionalization of CNTs has been explored as a way to improve CNTs stability, especially through the use of polydopamine (PDA) coatings that preserves CNTs intrinsic properties.[4,6,7] The introduction of catechol and amine groups from PDA to the pristine CNTs surface not only improves the dispersibility of CNTs in water-based preparation solutions, but also allows further functionalization of the CNTs surface with other functional groups.[16] The presence of the catechol groups could even allow the preparation of hybrid surfaces with metal promoters through chelation reactions, facilitating the interaction with metal matrices and increasing the range of application of CNTs on hybrid materials.[16]

Recent studies have described the successful use of PDA to improve CNT dispersion in aqueous solutions. Li *et al.* demonstrated its effectiveness as a support for metal and bimetallic nanoparticle synthesis (*e.g.*, Cu, Ni, Cu–Ni), promoting uniform nucleation and particle stabilization under thermal treatment.[17] Singh *et al.* reported improved aqueous stability and multifunctionality of PDA-coated CNTs, which support their reliable integration into metal matrices.[18] Devadas *et al.* further emphasized PDA's ability to modulate surface chemistry and bind metal ions, reinforcing its value in enhancing interfacial adhesion and electrical performance in CNT–metal nanocomposites.[19] Salomäki *et al.* showed that redox-active metals like Ce(IV), Fe(III), and Cu(II) enable fast PDA nanoparticle formation at low pH, but lead to differences in nitrogen content and metal incorporation, with Fe(III) showing the highest metal retention.[20] Duhain *et al.* developed a compression system for the preparation of CNT-metal composites with 40% CNT volume using an aqueous electrodeposition solution, without swelling of the CNT carpet, using oxidation and dopamine polymerization onto CNTs to introduce oxygen-containing functional groups and promote a uniform dispersion with enhanced copper wettability.[21] While the temperature coefficient of resistance of the composites improved compared to pure copper, swelling and depletion of copper were observed in the regions where mechanical failure occurred, causing a drop of the ampacity. The incorporation of nickel as a promoter phase between copper matrix and the CNTs proved to be successful, as no swelling was observed on the failure zone of the composites prepared with this metal.[21]

In this study, we explore how surface modification of CNTs with PDA, promoted by metal ions and modulated by pH and CNT length, affects polymerization behaviour, dispersion quality, and copper wettability. By integrating these parameters, we develop a strategy to engineer high-performance CNT–copper composites with improved interfacial bonding, aiming at lightweight, conductive materials for applications such as lightning strike protection.

Experimental

Sample nomenclature

The sample nomenclature used throughout this work is defined as follows: P and O correspond to pristine and oxidized CNTs, respectively. CNTs are functionalized with PDA at pH 3 or 8.5 were labelled CNT@PDA, followed by the pH value. For the samples functionalized with PDA in the presence of copper or nickel ions, the label CNT@PDACu or CNT@PDANi was used, followed once again by the value of pH at which the reaction occurred. Additionally, the use of 200 or 800 denotes the length of the CNTs, respectively 200 and 800 μm.

Method of preparation

The preparation of self-standing carpets using PDA-functionalized CNTs was achieved following an adapted procedure, previously published.[22] Commercial multi-walled CNTs were obtained from NanotechLabs, Inc., with distinguished 200 and 800 μm length. Dopamine hydrochloride, nitric acid (65%), nickel sulphate hexahydrate, copper sulphate pentahydrate, sodium hydroxide and PTFE membrane (Omnipore, 10 μm pore size) were bought from Sigma-Aldrich. Hydrochloric acid (37%, AnalaR NORMAPUR) was bought from VWR. Tris(hydroxymethyl)aminomethane was bought from Euromedex.

Carbon nanotube oxidation

100 mg of CNTs underwent treatment with 50% nitric acid in an ultrasonic bath for 30 minutes. Following recovery and wash, they were dispersed in ethanol and stored for further manipulation. The ultrasonic treatment was chosen to ensure even dispersion and uniform modification of CNTs, and nitric acid's effectiveness in enhancing surface functionality for subsequent applications.

Functionalization with PDA

After oxidation, CNTs were re-dispersed in a 0.5 mM of dopamine hydrochloride aqueous solution, and the dispersion was kept on an ultrasonic bath for 30 minutes to prevent aggregation of the CNTs and promote the bonding between the monomer and the functional groups formed on the CNTs surface. After that, a buffer solution of Tris-HCL pH 8.5 was added to the main dispersion to augment the pH and kick off the polymerization reaction of dopamine into polydopamine. The solution was kept under magnetic stirring at 750 rpm for 24 hours. At the end of the 24 hours, a 1 M solution of sodium hydroxide was added to the dispersion to further raise the pH, helping in the filtration of the functionalized CNTs. Following collecting and wash, CNTs were dispersed in ethanol and stored for further manipulation.

Functionalization with PDA in the presence of metal promoters

A methodology similar to the previous one was followed for the preparation of functionalized CNTs with PDA in the presence of copper or nickel ions, by adding to the dopamine solution copper sulphate pentahydrate or nickel sulphate hexahydrate so that the metal salt final concentration achieves 1.5 mM.

CNTs self-standing carpet preparation

For the preparation of the CNTs self-standing carpets, the dispersion of CNTs was passed through a vacuum filtration system paired with a PTFE 10 μm pore size filter membrane. Before the solute fully dried in the membrane, the carpet was peeled from the filter using tweezers and finally dried in atmospheric environment.

Characterization

Scanning electron microscopy (SEM) was used to assess the surface morphology and microstructure of the samples. The FEI Helio NanolabTM 650 SEM equipment was used at a working distance of 4 mm and an acceleration voltage of 2 kV. SEM images were acquired at various magnifications to investigate the surface characteristics, and the CNTs carpet thickness was obtained from treatment of multiple cross sections images of the samples.

X-ray photoelectron spectroscopy (XPS) was used to determine the elemental composition and chemical states of the samples, using the Cu 2p, Ni 2p, N 1s, C 1s, and O 1s photoelectron high resolution spectra. The Thermofisher Nexsa G2 XPS equipment was run with a monochromatic Al Kα X-ray excitation source operating at 120 W and using the 400 μm spot mode, all spectra were collected with a 20 eV pass energy. CasaXPS software version 2.3.26 was used to perform data quantification and peak fit operations.

Raman spectroscopy was employed to identify the degree of disorder in the CNT carbon lattice, which revealed vital information about its structural integrity after all the treatments done. An inVia Renishaw Raman spectrometer equipped with a 532 nm laser source was used. Spectra were collected over the range of 1200 to 1800 cm^{-1} with a 2400 l mm^{-1} granting resolution in a 5% power accumulation.

The electrical conduction mapping of the CNTs self-standing carpet was acquired by the mean of an MFP3D atomic force microscope (AFM) by Oxford Instrument, UK, operating in fast force mapping mode with an Asyelec-R2 Iridium coated tip. During the force-distance curves acquisition, the current was recorded from the output of a DLPCA-200 transimpedance amplifier (FEMTO, Germany) with a 1 V bias applied between the sample and the grounded tip. The sample laid on a stainless steel plate connected to the AFM adjustable bias output. The maximal value of current recorded during the force distance curve is used to create the conductive map. Two sets of mapping are obtained, a 45 × 45 μm^2 with a 32 × 32 $pxls^2$ at 2 μN setpoint to ensure a solid contact and to assess large areas, and a 10 × 10 μm^2 with a 256 × 256 $pxls^2$ at 200 nN for a finer mapping of the surface.

Thermogravimetric analysis was performed using the NETZSCH TG 209F1 Libra instrument, under an oxidative atmosphere composed of a mixture of O_2 and N_2 gases in a 20/80 ratio. The samples were placed in an open alumina crucible and the measurement was conducted from 30 °C to 800 °C at a heating rate of 10 °C per minute.

Results and discussion

CNTs have characteristically low reactivity due to absence of functional surface groups, which are required for dopamine bonding. This lack of reactive sites is the main cause of its hydrophobic behaviour. To address this, a preliminary treatment of the CNTs is necessary to introduce oxygen-containing reactive groups at the CNT outer surface, which improve the wettability and therefore the bonding of the CNTs surface with the monomer and polymer during functionalization. Among the different approaches that have been described for this end, a controlled acidic treatment, such as using a sulphuric and/or nitric acid mixtures to oxidize the CNTs for short periods of time (15 min to 48 h, with a maximum threshold of 2 days being established for CNTs self-standing carpet preparation), has proven its efficiency.[23–25]

In this study, we started by a mild oxidation step (involving the treatment of CNTs with nitric acid at room temperature and for 30 minutes) to ensure an improved dispersion stability of the treated nanotubes by charges repulsion.[26] While a low concentration of acidic sites is expected, a positive impact on the polymerization yield has already been reported.[27–29] Compared to stronger oxidation conditions, the mild oxidation process avoids the creation of CNTs lattice defects. SEM images of the pristine and oxidized CNTs, shown in Fig. 1a–c, revealed no significant morphological differences among the samples.

These results were further corroborated by XPS analysis, as the CNTs chemical composition was also unaffected by the treatment with nitric acid, as shown in Fig. 1h. The C 1s spectra remained mainly unchanged for both pristine and oxidized CNTs, supporting the controlled and selective character of the oxidation process, while it is observed in strong oxidation conditions an increase on the peak shoulder.[31] However, in our case there is no evolution in the asymmetric profile (peak tail shape) where the contributions of carbon bonding to oxygen are generally identified, nor significant alterations to the carbon sp^3 peak, suggesting limited functional group formation and minimal changes on the graphitic structure. Finally, some authors describe that a strong oxidation of CNTs by acidic treatment could lead to the removal of metallic particles, normally used as catalytic nuclei during CNT growth.[27,28] This particles were observed inside the CNTs during high-resolution transmission electron

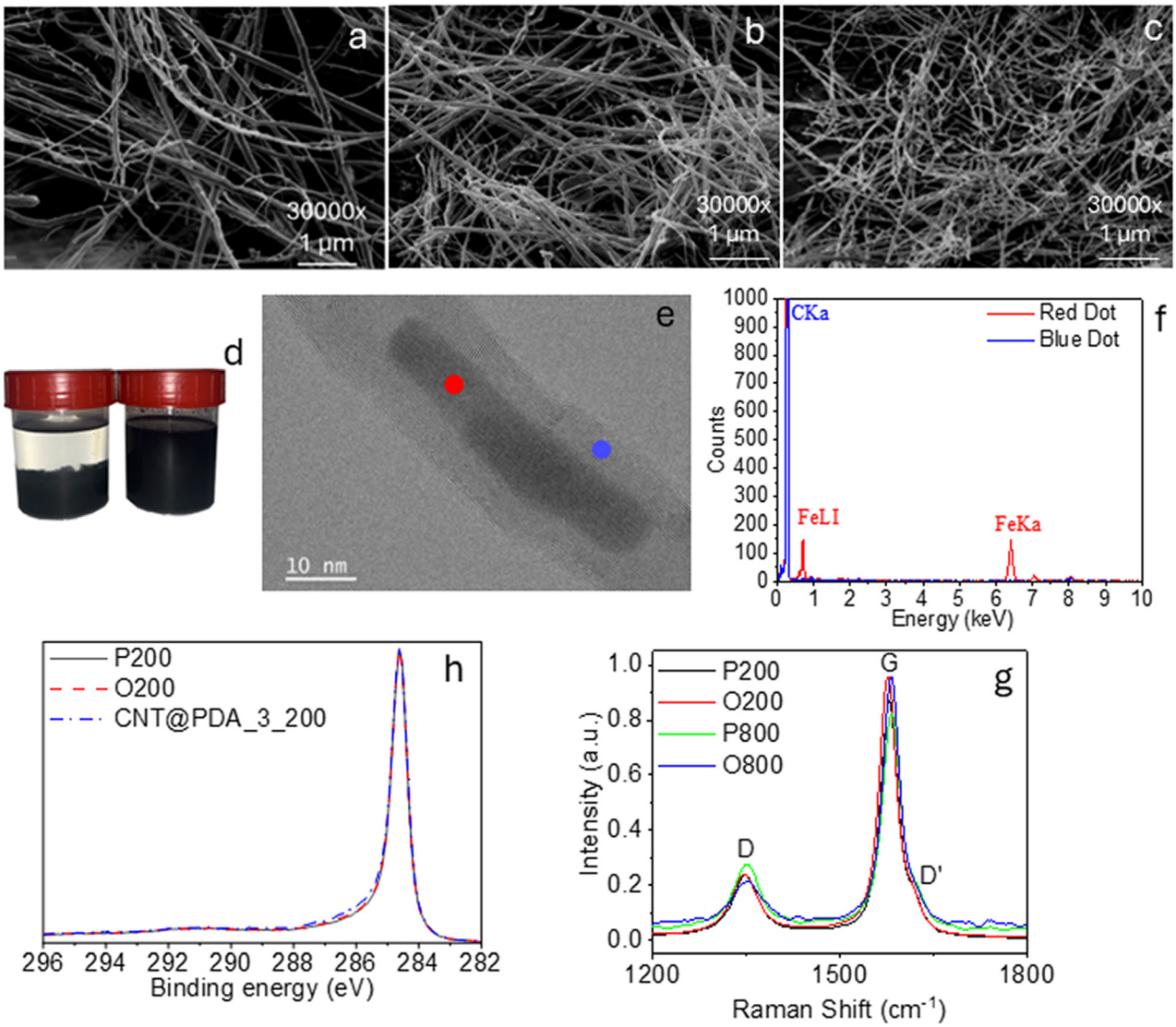

Fig. 1 Scanning electron microscopy images of pristine (a), oxidized (b) and PDA-functionalized (c) 200 μm CNTs. Picture (d) of dispersion of 200 μm CNTs functionalized with PDA at pH 3 (left) and pH 8.5 (right) after 48 h. Transmission electron microscopy image of an oxidized 200 μm CNT (e), and identification of two energy dispersive X-ray analysis areas, namely the CNT wall (blue dot) and catalytic particle (red dot) with corresponding spectrum (f). Raman spectroscopy spectra (g) of 200 and 800 μm pristine and oxidized CNTs. C 1s X-ray photoelectron spectroscopy (XPS) spectra of pristine (—), oxidized (- - -) and pH 3 PDA-functionalized (-·- - ·) 200 (h) μm CNTs.

microscopy (Fig. 1e), and analysing the area by energy-dispersive X-ray allowed us to identify those structures as iron clusters, confirming the absence of any severe modification of the CNTs (Fig. 1f). This is further observed when comparing the Raman spectra of pristine and oxidized CNTs, as there is no increase on the I_D/I_G ratio as well as the lack of the D′ peak (second order scattering defects on the graphitic layer), as shown in Fig. 1g.[27,29,30]

The next step focused on investigating CNTs-PDA interface. CNTs with two different lengths were functionalized using dopamine as monomer for PDA polymerization.[21] This process is kicked-off by the auto-oxidation reaction of dopamine in the presence of oxygen. However, this reaction is highly dependent on the pH of the environment, as at basic pH the catechol auto-oxidation reaction outcompetes the oxygen reduction, therefore favouring PDA formation.[21] In the presence of CNTs, PDA was polymerized at the optimal pH of 8.5. At this pH, polymerization is initiated by the oxidation of catechol to quinone, without triggering over-oxidation caused by excess hydroxyl ions. The pH also helps maintain a zwitterionic structure, which promotes oligomer stability.[23,32] A second polymerization was studied at pH 3. The dispersion of CNTs functionalized with PDA at a pH 8.5 showed a macroscopic stability until three weeks, while the CNTs functionalized with PDA at pH 3 dispersion went through a phase separation after 48 hours, as observed in Fig. 1d.

The presence of PDA in both samples was verified through the chemical characterization of the functionalized CNTs (Table 1). Comparing the composition of the pristine and

Table 1 Elemental composition based on XPS spectra of C 1s, O 1s, N 1s, Cu 2p and Ni 2p for 200 and 800 μm length pristine CNTs (named P in the table), oxidized CNTs (O), CNTs functionalized with PDA at pH 3 and 8.5 (CNT@PDA_3, CNT@PDA_8.5), and CNTs functionalized with PDA in the presence of copper and nickel ions at pH 3 and 8.5 (CNT@PDACu_3 and _8.5, CNT@PDANi_3 and _8.5). The abbreviation *na* (non-applicable) remarks the absence of a species

CNT length	Sample	C at%	O at%	N at%	Cu at%	Ni at%
200 μm	P	98.8	1.0	*na*	*na*	*na*
	O	98.1	1.6	*na*	*na*	*na*
	CNT@PDA_3	96.1	3.1	0.7	*na*	*na*
	CNT@PDA_8.5	84.2	11.2	4.0	*na*	*na*
	CNT@PDACu_3	88.0	8.3	1.1	1.3	*na*
	CNT@PDACu_8.5	67.6	21.6	7.2	3.0	*na*
	CNT@PDANi_3	64.6	24.3	4.6	*na*	6.5
	CNT@PDANi_8.5	49.8	30.8	4.5	*na*	14.9
800 μm	P	98.4	1.5	*na*	*na*	*na*
	O	98.6	1.2	*na*	*na*	*na*
	CNT@PDA_3	96.2	2.9	0.7	*na*	*na*
	CNT@PDA_8.5	77.1	16.0	6.6	*na*	*na*
	CNT@PDACu_3	92.1	5.8	1.2	0.8	*na*
	CNT@PDACu_8.5	67.3	21.1	8.2	3.2	*na*
	CNT@PDANi_3	62.5	26.2	5.4	*na*	6.1
	CNT@PDANi_8.5	52.2	28.9	5.2	*na*	13.6

oxidized CNTs to the one of CNTs functionalized with PDA, an increase in the oxygen and nitrogen atomic percentage is observed whatever the pH. This hints that the CNTs surface is coated with molecules containing these atoms after polymerization, likely polydopamine. The effect of the pH on the polymerization process is also confirmed in the elemental composition of the CNTs, as the percentage of oxygen and nitrogen is higher for the CNTs functionalized with PDA at a pH of 8.5, in accordance with the registers from literature.[24,25]

High resolution C 1s and N 1s XPS spectra of the samples processed at pH 3 and 8.5 are shown in Fig. 2. The components identified in the C 1s spectra of both CNTs functionalized at pH 3 and 8.5 can be identified as C═C (observed at binding energy (B.E.) of 284.5 eV), C–C/C–H (B.E. = 285.0 eV), C–O/C–N (B.E. = 286.4 eV), C═O/C═N (B.E. = 287.9 eV) and O═C–O–H (B.E. = 289.0 eV).[30,31] At an acidic pH, there is a decrease in the contributions of carbon–oxygen and carbon–nitrogen bonding. Furthermore, the absence of an increase in the shoulder of the C 1s spectrum peak suggests the polymerization yield is hindered at this pH, as observed in Fig. 1h. PDA is mainly composed of dopamine derived structures and indole/indoline structures, which could be identified in the N 1s core level spectra as secondary amine (B.E. = 400.0 eV), having the main contribution, and two other peaks related to $R–NH_3^+$ (B.E. = 401.6 eV) and tertiary amine (B.E. = 398.7 eV).[23,32] The high contribution of the secondary amine allows to identify the main polymer building block as indole/indoline structures formed by ring closure due to oxidation of the dopamine/dopamine quinone, which has also been previously reported by Hemmatpour *et al.*[11,12,32]

To confirm the pH effect on the polymerization of PDA on the surface of CNTs, thermogravimetric analysis was conducted (Fig. 3). The weight loss was followed as a function of the temperature under oxidative conditions. All degradation steps were identified using the derivative of the thermogravimetric curves, so that the temperatures corresponding to the key degradation points were extrapolated.

CNTs exhibited a significant thermal stability, displaying a one-step degradation process involving the breakage of the carbon lattice and the disruption of the π-conjugation, reaching a degradation temperature of 648 °C, regardless of length (Fig. 3a–c). Dopamine, on the other end, showed a multi-step process degradation with lower thermal stability when compared to CNTs. This process first involves the desorption of water molecules up to 240 °C, followed by the degradation of the catechol group until 310 °C and the amine group up to 370 °C, with the remaining carbonaceous material combusted up to 615 °C. Likewise, the PDA polymer follows a similar degradation pathway, characterized by the same steps but occurring at lower temperatures and with different weight contributions for each functional group. The observed temperature of degradation steps for both DA and PDA are in line with existing literature reports.[22,33]

When CNTs are functionalized with PDA, the degradation process is composed by two main steps. At lower temperatures, it is possible to identify a first degradation, which was associated with the polymer degradation due to its lower thermal stability. The degradation of polymeric functional groups is succeeded by the degradation of carbonaceous materials at elevated temperatures, wherein both the degradation of carbon nanotubes and the polymer carbon lattice is quantified. If we compare the derivative curve for pristine CNTs and CNTs@PDA, it is possible to understand a decrease in the temperature of degradation of the carbonaceous materials, as the adsorption of polymer on the surface of the CNTs causes the covering of the carbon lattice and therefore less entanglement between CNTs, resulting in a less thermally stable material.[34]

To assess the impact of the CNTs length on the polymerisation yield, we used the model designed by Peigney *et al.*,[35] that relates the number of walls and the outer diameter of the CNT with its specific surface area (SSA). The full calculation procedure and formula are provided in the SI. Based on this model and using the structural data obtained from TEM characterization of oxidized CNTs, we estimated the SSA of 83 $m^2\ g^{-1}$ and 59 $m^2\ g^{-1}$ for 800 μm and 200 μm CNTs respectively. The CNTs characteristics that were used to calculate the SSA are presented in Table 2. These values were obtained from the processing of TEM images of at least 5 individual CNTs per sample, which were included on the SI of this paper. For each CNT, ten measurements were taken along the length to determine an average number of walls and the observed variation.

It is important to clarify that the difference on SSA that we report arises from the structural characteristics of

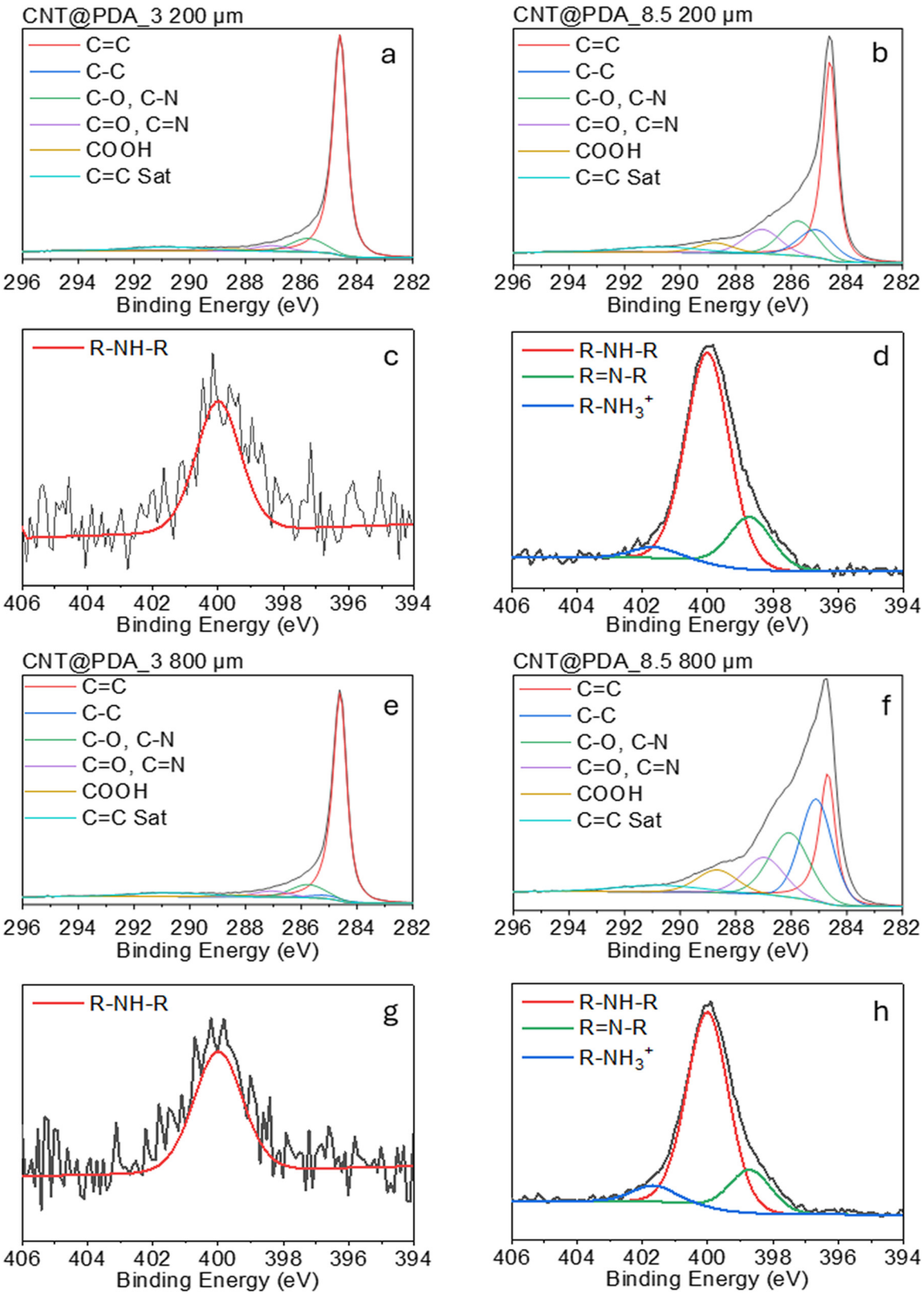

Fig. 2 High-resolution C 1s core level spectra of 200 μm CNTs functionalized with (a) PDA at pH 3 and (b) PDA at pH 8.5, 800 μm CNTs functionalized with (e) PDA at pH 3, (f) PDA at pH 8.5. High-resolution N 1s core level spectra of 200 μm CNTs functionalized with (c) PDA at pH 3 and (d) PDA at pH 8.5, 800 μm CNTs functionalized with (g) PDA at pH 3 and (h) PDA at pH 8.5.

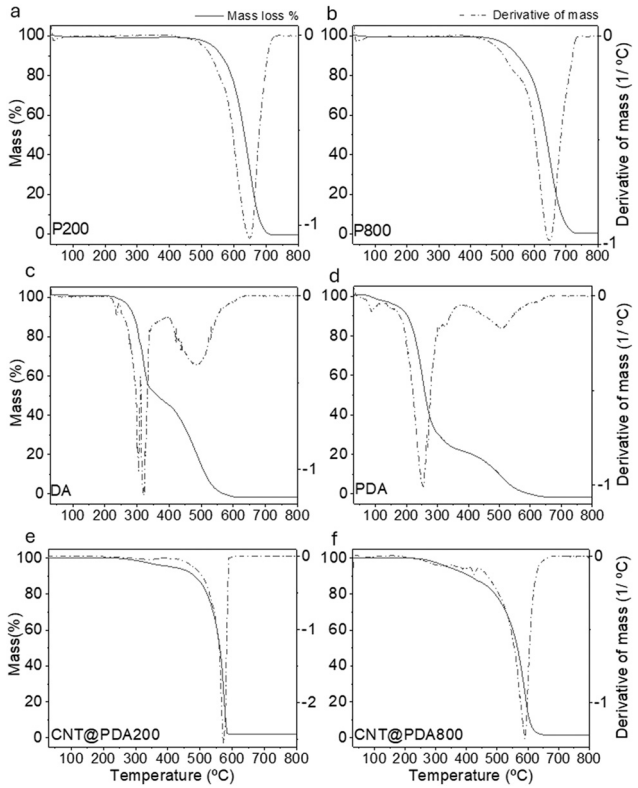

Fig. 3 Thermogravimetric analysis (TGA) showing weight loss percentage (solid line, left axis) and its derivative (dotted line, right axis) for pristine (a) 200 μm CNTs, (b) pristine 800 μm CNT, (c) dopamine monomer, (d) polydopamine, (e) 200 μm and (f) 800 μm CNTs functionalized with PDA at pH 8.5. The analysis was performed under nitrogen and oxygen atmosphere at 80/20 ratio, at a temperature range of the analysis between 25 °C and 800 °C, in a temperature slope of 30 °C per minute.

the CNTs, *i.e.* the fewer number of walls and the smaller diameter, and not the length of the CNTs itself. While the longer CNTs exhibited higher estimated SSA values, this result stems from their smaller average outer diameter and lower number of walls. These values are consistent with the expectations for multi-walled CNTs with large diameters and high wall numbers, for which the SSA typically lies well below 100 $m^2\ g^{-1}$, in contrast to the much higher values often reported for pristine single- or double-walled CNTs. Finally, according to literature, a lower number of walls, *i.e.* outer diameter, correlates with an augmented specific surface area (SSA), which consequently offers an increased number of reactive sites for the deposition of polydopamine (PDA), thereby facilitating a greater loading of uniformly applied polymeric coatings. This phenomenon elucidates the observed enhancement in the yield of polymerization, which is intrinsically linked to the elevated SSA characteristic of the 800 μm carbon nanotubes (CNTs).

PDA possesses insulating behaviour when compared to CNTs, so it is expected that PDA-functionalized CNTs show lower conductivity when compared to pristine or oxidized CNT.[17] This was confirmed by conductive AFM measurements shown in Fig. 4, which resumes the statistical treatment of the conductive mapping. It was observed that the longer CNTs showed a higher conductivity originated by the increased probability of an individual CNTs to bridge with its neighbours and reinforcing the conduction pathway. In general, the samples – pristine, oxidized, PDA-functionalized CNTs and PDA-functionalized CNTs in presence of copper ions – presented a heterogeneous behaviour, as observable by the data distributions. The average conductivity of the PDA-functionalized CNTs decreased when compared to its pristine nature, as shown by the decrease of the maximum absolute current in the histograms. The decrease of the average conductivity of the samples points to a greater and/or even more homogeneous distribution of PDA deposits on the surface of CNTs. These results support the hypothesis that the pH level has a significant role in PDA polymerization yield, since CNT samples functionalized with PDA at pH 8.5 demonstrated lower conductivity compared to samples functionalized at pH 3. Moreover, it can be seen in Fig. 5 that the intrinsic conductivity of the CNTs was not affected after the oxidative process.

Although PDA is intrinsically insulating and even locally reduces the conductivity of CNTs, its use in CNT-Cu composites has a more extensive purpose. Firstly, it has been shown that PDA improves CNT dispersibility and stability in aqueous media, which is essential for achieving uniform deposition during the controlled CNTs self-standing carpet elaboration step prior to electroplating. Moreover, PDA introduces functional groups, such as catechol and amines, which allow strong complexation bonding with metal ions like Cu^{2+} or Ni^{2+}. This enables uniform metal nucleation and growth along the CNT surface, promoting robust interfacial bonding with the copper matrix.[17,35,36] This improved interface is pivotal for minimizing contact resistance and enhancing both electrical and mechanical properties of the perspective CNT-metal composite. Hence, despite its insulating nature, PDA acts as a key interfacial layer that enhances the overall conductivity, durability, and thermal stability of the resultant composite.[17,34,36,37]

The presence of metal ions in the solution during CNTs functionalization can impact the PDA polymerization process. It has been described in literature that metal ions can act as coordination nuclei for PDA molecules in solution.[36,37] To

Table 2 Characteristics of CNTs used on specific surface area (SSA) calculation

Length (μm)	Diameter (nm)	Number of walls	Specific surface area ($m^2\ g^{-1}$)
200	45 ± 13	28	59
800	24 ± 10	23	83

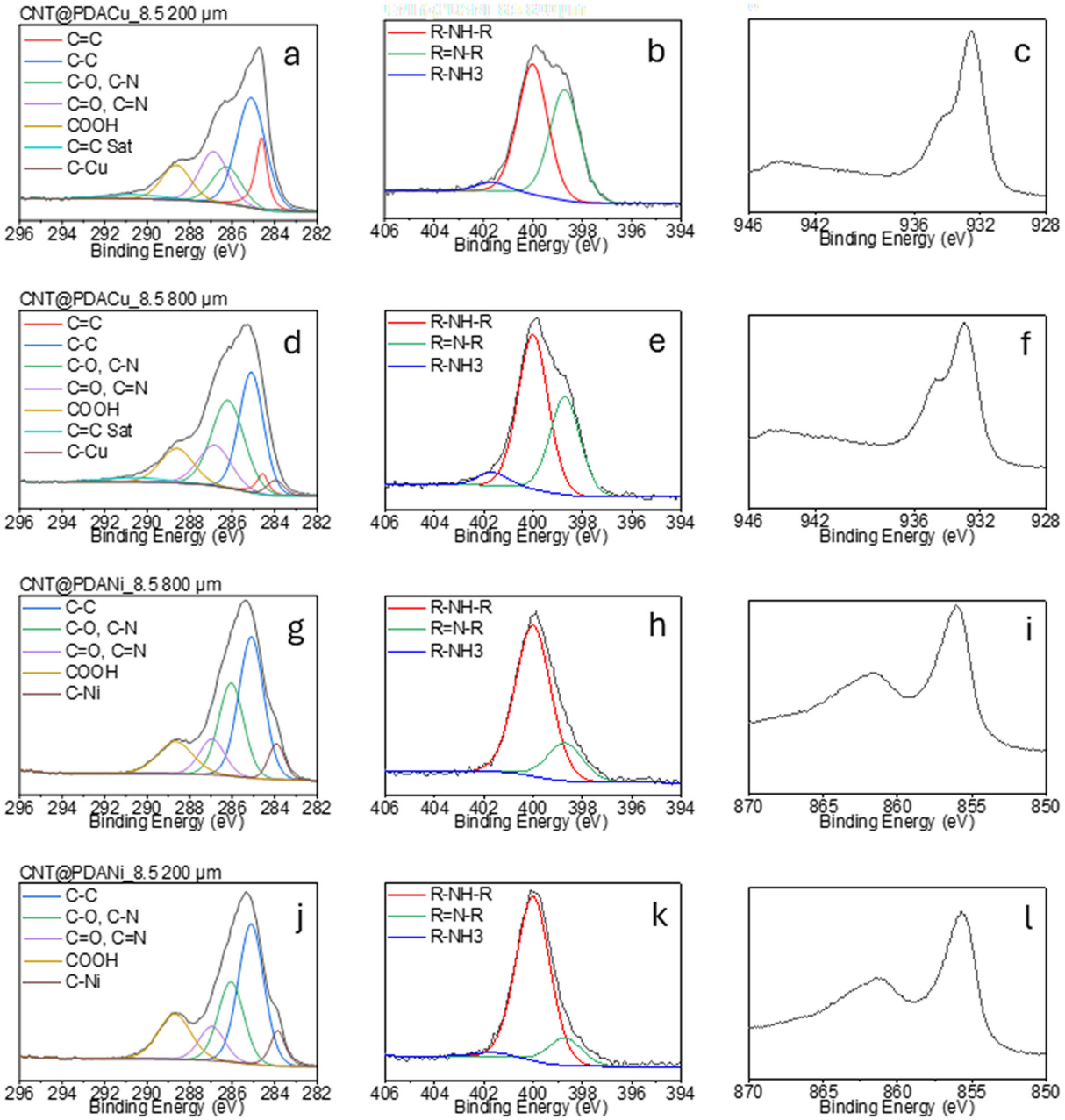

Fig. 4 High-resolution X-ray photoelectron spectroscopy (XPS) C 1s (a), N 1s (b) and Cu 2p (c) core level spectra of 200 μm CNTs functionalized with PDA in presence of copper sulphate at pH 8.5, C 1s (d), N 1s (e) and Cu 2p (f) core level spectra of 800 μm CNTs functionalized with PDA in presence of copper sulphate at pH 8.5, C 1s (g), N 1s (h) and Ni 2p (i) core level spectra of 200 μm CNTs functionalized with PDA in presence of nickel sulphate at pH 8.5, C 1s (j), N 1s (k) and Ni 2p (l) core level spectra of 800 μm CNTs functionalized with PDA in presence of nickel sulphate at pH 8.5.

address this matter, PDA polymerization was carried out in the presence of copper ions, because of their crucial role in the perspective CNTs-Cu composite preparation by enhancing the adhesion, promoting uniform copper deposition on CNTs surface and overcoming CNTs cuprophobicity.[14,38] Additionally, nickel ions were also considered in this study, as this metal has previously been reported to act as cuprophobicity mitigator.[11,12]

As shown in Table 1, the samples functionalized in the presence of metal promoters showed increased contributions of carbon binding to nitrogen and oxygen, suggesting an improvement on the polymerization yield (Fig. 4).[39–44] This hypothesis is further supported by the electrical behaviour of the samples depicted in Fig. 5, showing an decrease in electrical conductivity. This trend is linked to the role of the metal promoters on the chelation of solubilized polymer during PDA polymerization, which is believed to intensify the reaction and consequently lead to a higher polymerization yield. The N 1s core level spectra showed an increase on the

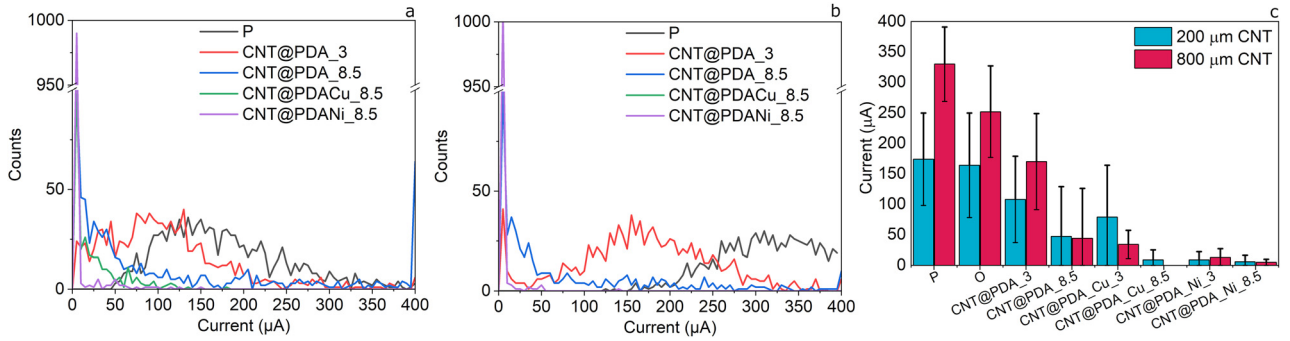

Fig. 5 Distribution of current measured by C-AFM for 200 (a) and 800 (b) μm pristine CTNs, CNTs functionalized with PDA at pH 3 and 8.5, and in the presence of copper and nickel ions. Weighted average current values (c) of 200 and 800 μm pristine and oxidized CNTs, as well as CNTs functionalized with PDA at pH 3 and 8.5, and as well in the presence of copper and nickel ions. Error bars represent the standard deviation from six independent measurements per sample.

contributions of R═N–R, which can be an indicator of trapping of simpler building blocks containing primary amines (amine and quinone), when compared to the contributions of the secondary amine present on the spectra of CNTs functionalized with PDA without metal promoters.

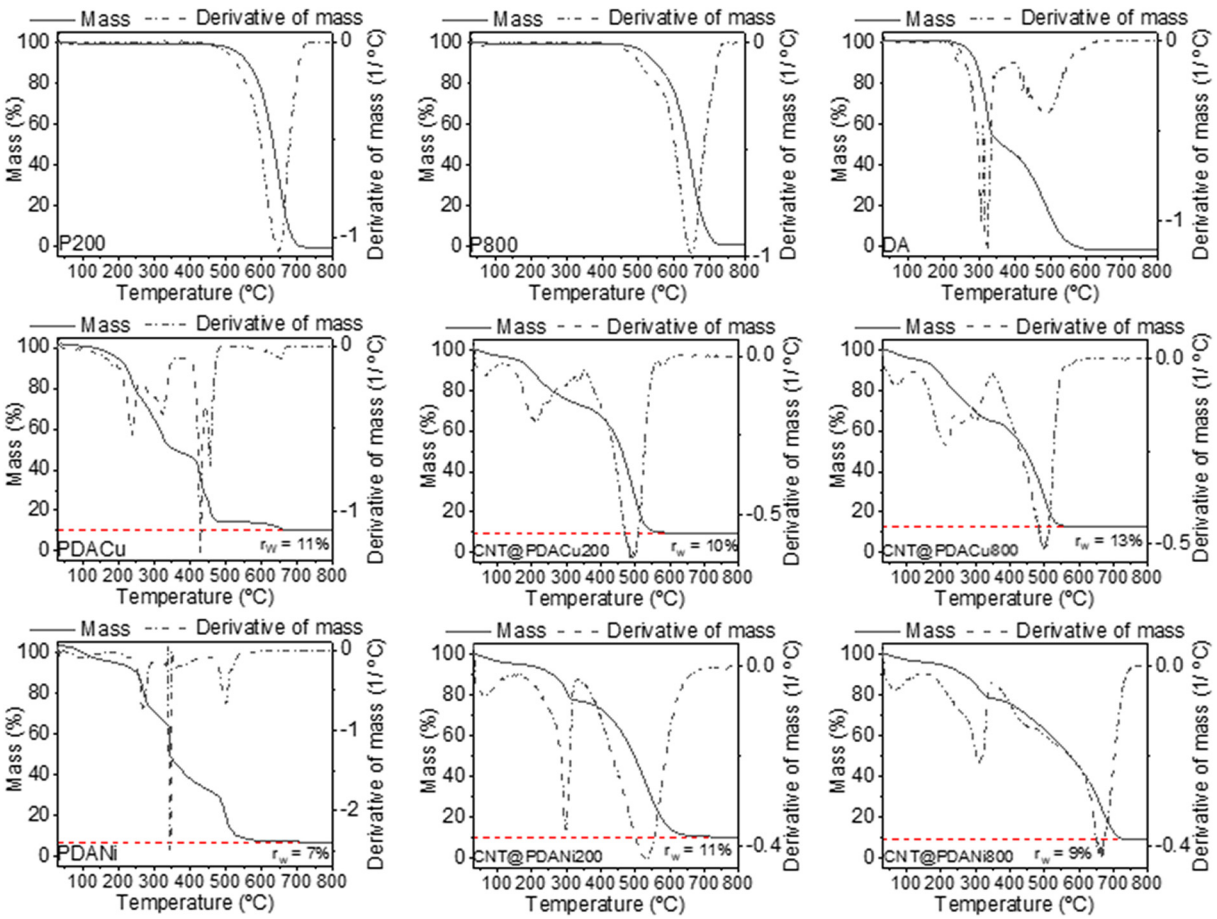

Fig. 6 Thermogravimetric analysis (TGA) (full line) and its derivative weight loss percentage (dotted line) curves for pristine 200 μm CNTs, pristine 800 μm CNT, dopamine monomer, polydopamine synthetized in the presence of copper sulphate at pH 8.5, 200 μm and 800 μm CNTs functionalized with PDA synthetized in the presence of copper sulphate at pH 8.5, polydopamine synthetized in the presence of nickel sulphate at pH 8.5, 200 μm and 800 μm CNTs functionalized with PDA synthetized in the presence of nickel sulphate at pH 8.5. Residual weight percentage after thermal degradation is also presented as the baseline of the TGA at dotted red. The analysis was performed under nitrogen and oxygen atmosphere at 80/20 ratio, at a temperature range of the analysis between 25 °C and 800 °C, in a temperature slope of 30 °C per minute.

The Ni 2p spectrum revealed a broad singlet peak at 855.9 eV and a satellite structure centred around 861.8 eV, attributed to the nickel hydroxide species. The copper spectrum showed two main peaks at 933.2 eV and 934.8 eV and their associated Cu^{2+} satellite features (B.E. = 948–936.0 eV range), attributed to copper oxide and hydroxide species respectively.[45–51] Literature reports suggest that metals can not only act as an activator on the autooxidation of catechol, competing with oxygen and secondary radicals, but also as a chelation agent responsible for formation of complexes with polymeric structures that are dispersed in solution during the polymerization.[36,37] This phenomenon is associated to higher PDA deposition yields, as the chelation of the dispersed polymer allows its linking to the already deposited film.[16] Chemical characterization by XPS indicated that copper and nickel hydroxide are present in the polymeric film, which is consistent with the side reaction between the metal sulphates and sodium hydroxide during the polymerization of PDA.[52]

The PDA polymerisation and the inclusion of metal promoters were investigated by thermogravimetric analysis of the PDA functionalized CNTs (Fig. 6). It showed that the polymer still follows a general multistep degradation process typical of complex polymers. The desorption of water molecules from the polymeric matrix is the first weight loss observed, which occurs until 255 °C. Like the monomer, the polymer suffers hydroxyl loss in a range of temperatures quite similar, in this case between 255 and 365 °C. The amine moiety of the polymer is degraded until temperatures of 495 °C, after which the carbon materials carbonization is observed. The main weight loss is associated to the degradation of graphitic lattice, at a temperature of 500 °C. Above 700 °C all carbonaceous materials have been degraded, and the remaining residues correspond to the metallic ions loaded in PDA.

Comparing the residual weight of the polymer synthesized in the presence of metal ions (PDACu and PDANi) with the corresponding functionalized CNTs introduced further insights into the effectiveness of polymerization and metal ion incorporation as dependent on the CNTs length. The values of residual weights correspond to residual non-volatile species that were entrapped in the polymeric matrix. However, it was observed that copper-related residual weight percentage (11%) is slightly higher than nickel one (7%), due to Cu-NH_2 chelation. This phenomenon will be further detailed on coming studies.

From the presented results, it can be inferred that in an acidic environment, both chemical and electrical characterizations indicate that the PDA polymerization is insufficient to change the CNTs surface chemistry or electrical properties. This is supported by the low nitrogen and oxygen content observed by XPS and a conductivity not very different from pristine CNTs one observed in the C-AFM measurements. In contrast, at basic pH, dopamine undergoes a more effective polymerization, resulting in higher PDA content loaded to the CNTs. This is confirmed by enhanced N and O contributions on XPS, a great weight loss in TGA, and a significant decrease in the conductivity with respect to pristine CNTs. This enhancement in polymerization is further boosted by the presence of metal ions during the polymerization process, that act as polymerization promoters. The samples functionalized with PDA in the presence of the metal promoters exhibited higher PDA content, as shown by the further reduction in conductivity observed in C-AFM, and the reinforced chemical shifts observed in XPS. The complementary results indicate a significant correlation between the pH-dependent polymerization process and the impact on the electrical performance of the functionalized CNTs thereby establishing the relevance of our methodology within the domain of electroplated copper–carbon composites.

Conclusions

This study unveils how the dopamine polymerization process on CNTs surface is affected by the presence of redox-active metal ions (Cu^{2+}, Ni^{2+}) and the pH environment (acidic *versus* mildly alkaline), with focus on enabling an effective surface functionalization for improved wettability and metal affinity of CNTs.

A mild nitric acid oxidation was shown to preserve the structural integrity of the CNTs while introducing reactive sites. It is noted that longer CNTs presented a higher specific surface area (SSA), due to their lower number of walls and smaller diameter when compared to the shorter CNTs used in this study. Our results confirmed that pH 8.5 optimally supports dopamine polymerization by promoting catechol oxidation, which is suggested to create oligomer stability and a more effective functionalization of the CNT surface. This phenomenon was further intensified in the presence of metal ions promoters. Copper ions, in particular, acted as chelating agents, bridging solubilized PDA and deposited PDA films, while nickel also facilitated wettability improvements, whose mechanistic role still requires further investigation.

These findings emphasize that the precise tuning of the oxidation level, CNT morphology, reaction pH and metal ion content allows for a fine control over the polymerization efficiency, PDA yield, and overall interface chemistry. This control is the key parameter to mitigate CNT hydrophobicity and cuprophobicity, both critical gate keys in the perspective to achieve robust interfacial bonding in CNT-Cu composites for high ampacity applications.

Finally, we report the formation of an intermediary species with a carbide bonding nature between carbon and metals ions used during functionalization. This suggests a strong interfacial interactive effect, with implications for enhancing composite stability and electrical behaviour. Overall, this work provides a foundational strategy for tailoring the CNTs surface *via* pH-metal assisted PDA polymerization, offering pathways toward high-performance, lightweight composited with controlled electrical,

mechanical, and interfacial properties for advanced technological applications.

Conflicts of interest

There are no conflicts to declare.

Data availability

Data for this article, including XPS and TGA raw files, CNTs structural properties and Raman data are available at Science Data Base at **https://doi.org/10.57760/sciencedb.28231**.

Supplementary information is available. See DOI: **https://doi.org/10.1039/d5re00209e**.

Acknowledgements

We thank H. Mallek, T. Devahif and G. Jacqmin for the scientific insight and proofreading, and B. Marcolini for TGA data acquisition.

References

1 S. Bhadra, M. Rahaman and P. Noorunnisa Khanam, in *Carbon-Containing Polymer Composites*, ed. M. Rahaman, D. Khastgir and A. K. Aldalbahi, Springer Singapore, Singapore, 2019, pp. 397–455.
2 I.-Y. Jeon, D. Wook, N. Ashok and J.-B. Baek, in *Carbon Nanotubes-Polymer Nanocomposites*, ed. S. Yellampalli, InTech, 2011.
3 P. Eskandari, Z. Abousalman-Rezvani, H. Roghani-Mamaqani and M. Salami-Kalajahi, *Adv. Colloid Interface Sci.*, 2021, **294**, 102471.
4 R. Dubey, D. Dutta, A. Sarkar and P. Chattopadhyay, *Nanoscale Adv.*, 2021, **3**, 5722–5744.
5 C. Zhang, L. Li, Y. Xin, J. You, J. Zhang, W. Fu and N. Wang, *Polymer*, 2021, **14**, 110.
6 A. M. Díez-Pascual, *Macromol*, 2021, **1**, 64–83.
7 Z. Spitalsky, D. Tasis, K. Papagelis and C. Galiotis, *Prog. Polym. Sci.*, 2010, **35**, 357–401.
8 M. Gagné and D. Therriault, *Prog. Aerosp. Sci.*, 2014, **64**, 1–16.
9 A. Larsson, *C. R. Phys.*, 2002, **3**, 1423–1444.
10 R. A. Matula, *J. Phys. Chem. Ref. Data*, 1979, **8**, 1147–1298.
11 A. Fediai, D. A. Ryndyk, G. Seifert, S. Mothes, M. Claus, M. Schröter and G. Cuniberti, *Nanoscale*, 2016, **8**, 10240–10251.
12 K. Z. Milowska, M. Ghorbani-Asl, M. Burda, L. Wolanicka, N. Ćatić, P. D. Bristowe and K. K. K. Koziol, *Nanoscale*, 2017, **9**, 8458–8469.
13 R. M. Sundaram, A. Sekiguchi, M. Sekiya, T. Yamada and K. Hata, *R. Soc. Open Sci.*, 2018, **5**, 180814.
14 C. Subramaniam, T. Yamada, K. Kobashi, A. Sekiguchi, D. N. Futaba, M. Yumura and K. Hata, *Nat. Commun.*, 2013, **4**, 2202.
15 R. Sundaram, T. Yamada, K. Hata and A. Sekiguchi, *Mater. Today Commun.*, 2017, **13**, 119–125.
16 A. Mercadante, V. Campisciano, A. Morena, L. Valentino, V. La Parola, C. Aprile, M. Gruttadauria and F. Giacalone, *Eur. J. Org. Chem.*, 2022, **2022**, e202200497.
17 H. Li, J. Xi, A. G. Donaghue, J. Keum, Y. Zhao, K. An, E. R. McKenzie and F. Ren, *Sci. Rep.*, 2020, **10**, 10416.
18 I. Singh, G. Dhawan, S. Gupta and P. Kumar, *Front. Microbiol.*, 2021, **11**, 607099.
19 B. Devadas, C. C. Chang and T. Imae, *J. Taiwan Inst. Chem. Eng.*, 2019, **102**, 378–386.
20 M. Salomäki, T. Ouvinen, L. Marttila, H. Kivelä, J. Leiro, E. Mäkilä and J. Lukkari, *J. Phys. Chem. B*, 2019, **123**, 2513–2524.
21 A. Duhain, G. Lamblin and D. Lenoble, *RSC Adv.*, 2021, **11**, 40159–40172.
22 H. Xiao, C. Tao, Y. Li, X. Chen, J. Huang and J. Wang, *Nanomaterials*, 2018, **8**, 854.
23 J. Liebscher, *Eur. J. Org. Chem.*, 2019, **2019**, 4976–4994.
24 M. T. Cortés, C. Vargas, D. A. Blanco, I. D. Quinchanegua, C. Cortés and A. M. Jaramillo, *J. Chem. Educ.*, 2019, **96**, 1250–1255.
25 V. Ball, D. D. Frari, V. Toniazzo and D. Ruch, *J. Colloid Interface Sci.*, 2012, **386**, 366–372.
26 K. Esumi, M. Ishigami, A. Nakajima, K. Sawada and H. Honda, *Carbon*, 1996, **34**, 279–281.
27 L. Lavagna, M. Bartoli, D. Suarez-Riera, D. Cagliero, S. Musso and M. Pavese, *ACS Appl. Nano Mater.*, 2022, **5**, 6671–6678.
28 L. Lavagna, R. Nisticò, S. Musso and M. Pavese, *Mater. Today Chem.*, 2021, **20**, 100477.
29 S. Osswald, M. Havel and Y. Gogotsi, *J. Raman Spectrosc.*, 2007, **38**, 728–736.
30 W. M. Silva, H. Ribeiro, L. M. Seara, H. D. R. Calado, A. S. Ferlauto, R. M. Paniago, C. F. Leite and G. G. Silva, *J. Braz. Chem. Soc.*, 2012, **23**, 1078–1086.
31 B. R. C. De Menezes, F. V. Ferreira, B. C. Silva, E. A. N. Simonetti, T. M. Bastos, L. S. Cividanes and G. P. Thim, *J. Mater. Sci.*, 2018, **53**, 14311–14327.
32 H. Hemmatpour, O. De Luca, D. Crestani, M. C. A. Stuart, A. Lasorsa, P. C. A. Van Der Wel, K. Loos, T. Giousis, V. Haddadi-Asl and P. Rudolf, *Nat. Commun.*, 2023, **14**, 664.
33 M. R. De Guzman, C. K. A. Andra, M. B. M. Y. Ang, G. V. C. Dizon, A. R. Caparanga, S.-H. Huang and K.-R. Lee, *J. Membr. Sci.*, 2021, **620**, 118881.
34 X. Li, Y. Liu, S. Wang, Y. Zhang, F. Liu and J. Han, *Colloids Surf., A*, 2021, **631**, 127721.
35 A. Peigney, C. Laurent, E. Flahaut, R. Bacsa and A. Rousset, *Carbon*, 2001, **39**, 507–514.
36 F. Bernsmann, V. Ball, F. Addiego, A. Ponche, M. Michel, J. J. D. A. Gracio, V. Toniazzo and D. Ruch, *Langmuir*, 2011, **27**, 2819–2825.
37 M. J. Sever and J. J. Wilker, *Dalton Trans.*, 2006, 813–822.
38 E. Kazimierska, E. Andreoli and A. R. Barron, *J. Appl. Electrochem.*, 2019, **49**, 731–741.
39 Y. Goto, K. Taniguchi, T. Omata, S. Otsuka-Yao-Matsuo, N. Ohashi, S. Ueda, H. Yoshikawa, Y. Yamashita, H. Oohashi and K. Kobayashi, *Chem. Mater.*, 2008, **20**, 4156–4160.

40 S. Liu, Z. Yu, C. Lu, Y. Wang, F. Sun, Z. Sun, Y. Liu, C. Shi and A. Wang, *Fuel*, 2023, **334**, 126763.
41 Y. Yao, Z. Yu, C. Lu, F. Sun, Y. Wang, Z. Sun, Y. Liu and A. Wang, *Renewable Energy*, 2022, **197**, 69–78.
42 C. Lu, Y. Wang, R. Zhang, B. Wang and A. Wang, *ACS Appl. Mater. Interfaces*, 2020, **12**, 46027–46036.
43 S. Sinharoy and L. L. Levenson, *Thin Solid Films*, 1978, **53**, 31–36.
44 B. C. Bayer, D. A. Bosworth, F. B. Michaelis, R. Blume, G. Habler, R. Abart, R. S. Weatherup, P. R. Kidambi, J. J. Baumberg, A. Knop-Gericke, R. Schloegl, C. Baehtz, Z. H. Barber, J. C. Meyer and S. Hofmann, *J. Phys. Chem. C*, 2016, **120**, 22571–22584.
45 M. L. Farquhar, J. M. Charnock, K. E. R. England and D. J. Vaughan, *J. Colloid Interface Sci.*, 1996, **177**, 561–567.
46 M. C. Biesinger, *Surf. Interface Anal.*, 2017, **49**, 1325–1334.
47 L. S. Dake, D. E. King and A. W. Czanderna, *Solid State Sci.*, 2000, **2**, 781–789.
48 M. C. Biesinger, B. P. Payne, A. P. Grosvenor, L. W. M. Lau, A. R. Gerson, R. St and C. Smart, *Appl. Surf. Sci.*, 2011, **257**, 2717–2730.
49 M. C. Biesinger, L. W. M. Lau, A. R. Gerson, R. St and C. Smart, *Appl. Surf. Sci.*, 2010, **257**, 887–898.
50 M. C. Biesinger, B. P. Payne, L. W. M. Lau, A. Gerson, R. St and C. Smart, *Surf. Interface Anal.*, 2009, **41**, 324–332.
51 A. P. Grosvenor, M. C. Biesinger, R. St, C. Smart and N. S. McIntyre, *Surf. Sci.*, 2006, **600**, 1771–1779.
52 Y. Cudennec, A. Lecerf and Y. Gérault, *Eur. J. Solid State Inorg. Chem.*, 1995, **32**, 1013–1022.